AD-A111 944 FOREIGN TECHNOLOGY DIV WRIGHT-PATTERSON AFB OH F/G 20/5
LASER JOURNAL (SELECTED ARTICLES).(U)
FEB 82
UNCLASSIFIED FTD-ID(RS)T-1390-81 NL

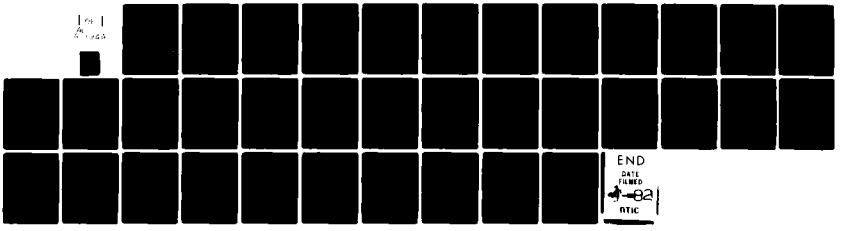

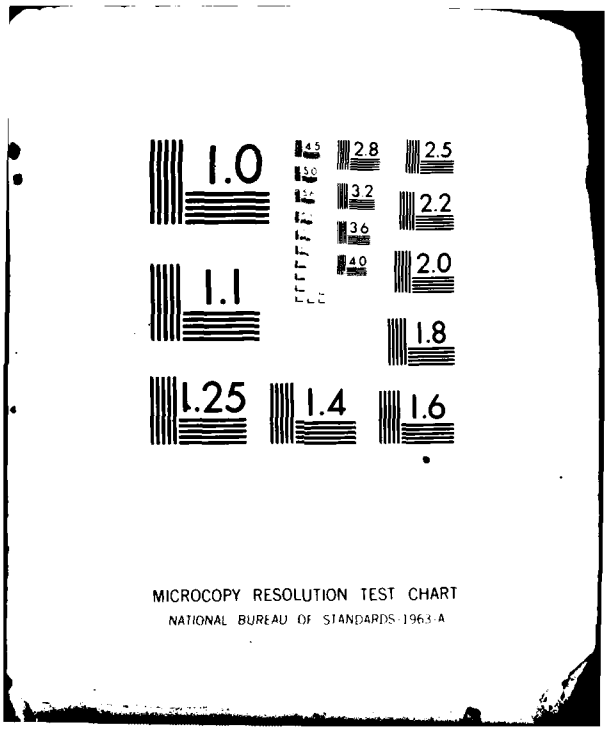
1.0
1.1
1.25
1.4
1.6
1.8
2.0
2.2
2.5
2.8
3.2
3.6
4.0
4.5
5.0
MICROCOPY RESOLUTION TEST CHART
NATIONAL BUREAU OF STANDARDS-1963-A

(2)

AD A111944

DTIC FILE COPY

FTD-ID(RS)T-0556-81

FOREIGN TECHNOLOGY DIVISION

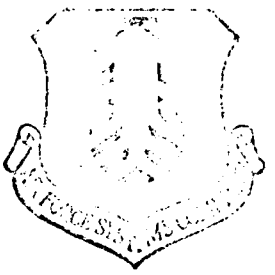

LASER JOURNAL

(Selected Articles)

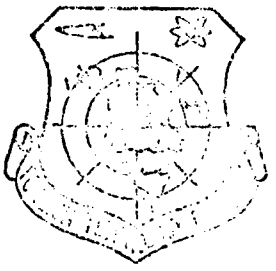

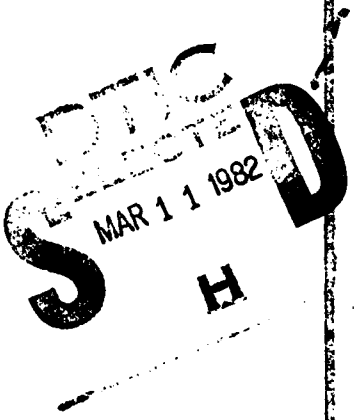

Approved for public release;
distribution unlimited.

EDITED TRANSLATION

FTD-ID(RS)T-1390-81 12 February 1982

MICROFICHE NR: FTD-82-C-000181

LASER JOURNAL (Selected Articles)

English pages: 33

Source: Laser Journal, Vol. 8, Nr. 1, 1981, pp. 5-9; 10-13; 18-20; 47-48

Country of origin: China
Translated by: LEO KANNER ASSOCIATES
F33657-81-D-0264
Requester: FTD/TQTD

PREPARED BY.

TRANSLATION DIVISION
FOREIGN TECHNOLOGY DIVISION
WP-AFB, OHIO.

Table of Contents

EFFECT OF THERMAL DEFORMATION IN MIRRORS ON RESONATOR PARAMETERS

Zhang Xinchun, Sun Hongjia, and Guo Gongjian
Shanxi University
Submitted 4 March 1980

Influence of thermal deformation in mirrors upon the resonator parameters is discussed. In designing a high power laser and a folded-resonator CO_2 laser in particular, it must be considered in advance as much as possible.

When laser power is increased, thermal deformation in mirrors due to absorption wearing is more apparent; this deformation becomes an important factor, affecting laser resonator parameters (in particular, more strongly folded CO_2 lasers). So this effect should be considered.

1. Experimental Details

We performed experiments with a 2-meter V-type folded CO_2 laser. Besides the output mirror, all reflection mirrors were made of ordinary optical glass on the base plates. An infrared-focus-adjusting automatic collimator was used to measure (from the back of mirrors) the variation in the radius of curvature. It was found that after laser operation, there was an apparent change in the glass [illegible]. When the backs of the mirrors were coated with [illegible] the difference between the front and back surfaces of mirrors was [illegible] the change of curvature radius (front surface adjusted to

[illegible] (with time) of the [illegible] of the [illegible] laser beam burned a circle mark on the [illegible] plate, as shown in figure 1. The width of spot [illegible] values [illegible] 30 seconds and 1 minute.

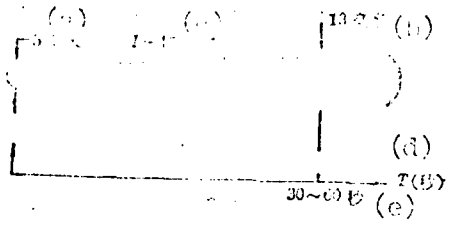

Fig. 1. Changes (with time) of laser output light-spot sizes.
Key: (a) 5 millimeters; (b) 13 millimeters; (c) 1.45 millimeters; (d) T (seconds); (e) 30-60 seconds.

We recommend that the difference in the light-spot sizes between the calculated value based on the cavity theory and the initial light spot at t=0 is caused by the lens-like effect of the working gas. The reason why the light spot slowly broadened with time is mainly caused by thermal deformation. Since the settling time of the lens-like effect of the gas can be estimated from the characteristic time during which the gas molecules diffuse from the center (of laser discharge tube) to the tube wall [1], and the estimated $\tau_{diffusion} \approx 0.1$ second applies to the working gas of CO_2 laser, it is apparent that the settling time of the lens-like effect (of gas) can be considered as instantaneous. The 30-second period in the experiments represents the settling time of the thermal deformation of the mirror.

Although the lens-like effect of the gas is apparent in a CO_2 laser tube [illegible] lines, the focal distance measured in experiments was more than [illegible] feet. However, in the above experiments, there were considerable changes with time in the light-spot sizes. This can be [illegible] by the effect of laser resonator caused by [illegible] thermal deformation is much more important than the thermal expansion effect. Therefore, [illegible] is relatively [illegible].

II. [illegible]

The thermal conductivity of the end plate of a mirror (in a CO_2 laser) is quite high, so the inner surface of the mirror can be generally considered as an isothermal surface. By the same token, the outer surface of the mirror also is kept at a certain constant temperature. Neglecting the small amount of heat carried away by the discharge tube wall, under the condition of thermodynamic equilibrium, the heat absorbed by the inner surface of the mirror per unit time should be equal to the heat carried away by heat conduction through the mirror per unit of time.

$$P(1-r) = 4.18\beta\left(\frac{\partial T}{\partial z}\right)S \approx 4.18\beta\frac{\Delta T}{d}S$$

In the above one-dimensional thermal conduction equation, P represents power in the laser chamber; r is the reflectivity of mirror; β is the coefficient of thermal conductivity of the mirror base plate, estimated at β=0.002 caloric per centimeter-second-degree; $\partial T/\partial z$ represents the temperature gradient along the direction of tube axis, approximately considered as $(\partial T/\partial z)_{\text{av}}(\Delta T/d)$; ΔT is the average temperature difference between the inner and outer surfaces of the mirror; d is the mirror thickness; and S is the mirror area (approximately equal to the cross-sectional area of the discharge tube). From the above equation, we derive

$$\Delta T \approx 120P(1-r)\frac{d}{S} = 120(1-r)\frac{Wd}{Si} \quad (1)$$

In the equation, W is the laser output power and t is the transmissivity of the output window.

As shown in Fig. 2, R is the radius of curvature of the concave lens. At the axis, the incident radius vectors are drawn from O (the center of curvature) toward the mirror; the included angle between the two radius vectors is ϕ. The curve sector l' at the outer surface of the mirror does not vary because of the constant cooling-water temperature. At the inner surface of mirror, an increase of ΔT in temperature is caused by the absorption of light energy. The curve sector was increased from l to $l'=(1+\alpha\Delta T)l$. In the equation, α represents the thermal [illegible] coefficient of the mirror base plate; for I_0 optical glass, α=90x10^{-7} [illegible]. After deformation, the [illegible] of curvature (of sphere) was R' and the [illegible] was diminished to r'. By [illegible] relationship, we can [illegible]:

$$R' = \frac{l'}{\varphi} = \frac{l(1+\alpha\Delta T)}{\frac{l}{R}\alpha\Delta T} = \frac{R(1+\alpha\Delta T)}{d}$$

$$\approx \frac{Rd}{R\alpha\Delta T} \qquad (2)$$

If the mirror is a plane lens, then

$$R' \approx -\frac{d}{\alpha\Delta T} \qquad (2)'$$

We can see that thermal deformation increases the radius of curvature of concave lens and changes a plane lens into a convex lens. The possible variation in the radius of curvature (of mirror) should be considered before designing a laser resonator. We call this a compensation design compensating for the thermally deformed resonator of the mirror.

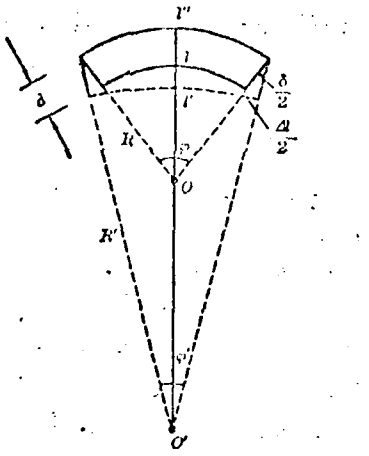

Fig. 2. Thermal deformation of mirror.

III. Effect on Resonator Parameters of Mirror Thermal Deformation

(A) Effect on straight cavity

In a straight cavity with length l and mirrors with radii of curvatures R_1 and R_2, for the output mirror R_1 as its thermal conductivity is relatively high

[illegible] which is:

$$g_1' = 1 - \frac{L}{R_1},$$

$$g_2' = \left(1 - \frac{L}{R_2}\right) - \frac{120\alpha L(1-\gamma)W}{St} = g_2 - MW,$$

In the equation, $M = \frac{120\alpha L(1-\gamma)}{St}$,

For a given mirror, M is a constant. We can see that the parameter g always linearly decreases algebraically with W. Thus, the laser output light-spot becomes:

$$\omega' = \sqrt{\frac{L\lambda}{\pi}}\left[\frac{g_2'}{g_1'(1-g_1'g_2')}\right]^{\frac{1}{4}} = \sqrt{\frac{L\lambda}{\pi}}\left\{\frac{g_2 - MW}{g_1[(1-g_1g_2) - g_1MW]}\right\}^{\frac{1}{4}}.$$

(B) Effect on folded chamber

Since the number of lenses is increased, the effect of mirror thermal deformation on parameters is much more involved than for a straight chamber. By taking as an example a relatively simple V-type folded chamber as shown in Fig. 3, when $a_1=a_2=a$ and $R_1=\infty$ (output of plane lens), the parameters of the equivalent chamber are derived as:

$$\begin{cases} N = \dfrac{a^2}{2\lambda L\left(1-\dfrac{L}{R_3}\right)} \\ G_1 = 1 - \dfrac{2L}{R_3} \\ G_2 = 1 - \dfrac{2L}{R_3} - \dfrac{2L}{R_3}\left(1-\dfrac{L}{R_3}\right) \end{cases}$$

When the chamber parameters become (after mirror thermal deformation) as follows:

$$\begin{cases} N' = 2AL\left[\left(1-\frac{e^*}{R_3}\right)+4MW\right] \\ G_1' = \left(1-\frac{2L}{R_2}\right)+4MW \\ G_2' = \left[\left(1-\frac{2L}{R_2}\right)-\frac{2L}{R_2}\left(1-\frac{L}{R_3}\right)\right] \\ \quad +2M\left[\left(3-\frac{2L}{R_2}\right)-\frac{L}{R_3}\right]W \\ \quad +4M^2W^2 \end{cases}$$

By using the correspondence relationship for the equivalent chamber G parameters and g parameters, we derived the following:

$$\begin{cases} g_1' = g_1 = 1 \\ g_2' = \left[\left(1-\frac{2L}{R_2}\right)+4MW\right]\left\{\left[\left(1-\frac{2L}{R_2}\right)\right.\right. \\ \quad \left.\left.-\frac{2L}{R_2}\left(1-\frac{L}{R_3}\right)\right]\right. \\ \quad +2M\left[\left(3-\frac{2L}{R_2}\right)-\frac{L}{R_3}\right]W \\ \quad \left.+4M^2W^2\right\} \end{cases} \tag{3}$$

From the above equations, the parameter G (or g) of the folded chamber also increases simple-harmonically with the laser output power W; however, the variation is much more apparent than for the straight chamber. The Fresnel number N decreases simple-harmonically with W; i.e., the mirror thermal deformation always lowers the Fresnel number. Particularly noteworthy is the fact that there is a fairly close relationship between the Fresnel number for the straight chamber and the radius of curvature (R_2) of the folded mirror. The decrease in the Fresnel number is mainly caused by thermal deformation of the folded mirror. Therefore, when designing the folded chamber it is very important to properly select the radius of curvature of related mirrors. From the simple harmonic variation of chamber parameters with the laser output power W, thermal deformation of mirror can change a steady chamber into an unsteady chamber. Conversely, it is also possible to change an excessively concentrating unsteady chamber into a steady working chamber.

If the effect of the gas beam-like effect is neglected for the moment, the radius of the curved line typed of the TEM$_{00}$ mode coming from laser output is

$$\omega = \sqrt{\frac{2A}{L}\left[1 - \frac{d}{g}\right]} \qquad (4)$$

In this equation, d is the width of the cathode of the V-type folded chamber. We obtain

$$L = \frac{2A\left[\left(1-\frac{L}{R_1}\right)+BMB'\right]}{\left[\left(1-\frac{2L}{R_3}\right)+BMB'\right]} \qquad (5)$$

r_2' is given in Equation (2).

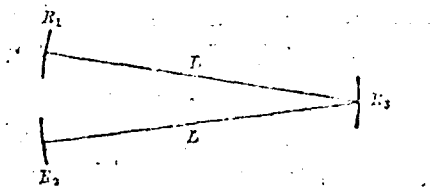

Fig. 3. V-type folded resonator

IV. Proof and Revision

Then the folded chamber shown in Fig. 3, select different combinations of the mirrors; an experiment is conducted to prove the theoretical calculations above. Assume L=2 meters, S=10 centimeters, d=0.5 centimeter, and t=45 percent, and $(1-\tau)$=1.4 percent. From calculations, M=6.72×10^{-4}. By applying plan number 1, $R_2=R_1=\infty$, R_3=40 meters, and r_1r_2=0.36<1; the cavity is a steady cavity. However, when W=1000 watts, $r_1'r_2'$=1.209>1, the working chamber becomes an unsteady chamber because of thermal deformation. With this type of mirror combination (in a laser), the optimal laser power is less than 100 watts; moreover, when the discharge current is increased from 20 to 40 milliamperes, the laser output power has no apparent change. By slightly plying mirrors manually to change the cavity mode, the output power also has no apparent change. This phenomenon reveals that there is very considerable loss in the cavity; this loss rapidly increases with increase in laser output power. Therefore, the output power becomes saturated (see Fig. 8). However, when plan number 2 is applied, $R_2=\infty$, R_3=10 meters, L=5 meters, $r_1'r_2'$=0.9 <1; the cavity is an unstable cavity. When W=10 watts, $r_1'r_2'$=0.706<1; the

[illegible] (3), (4) and (5), calculate for parameters of the two [illegible] the length l_0 of the equivalent cavity and the cavity perturbation η due to the corrugated dimensions of light spots in the TEM_{00} and TEM_{10} modes. The values are listed in Table 1.

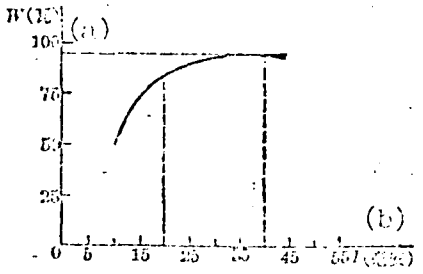

Fig. 4. Output power exhibits saturation during thermal deformation as the steady cavity becomes a wearing cavity (unstable).
Key: (a) (watts); (b) (milliamperes).

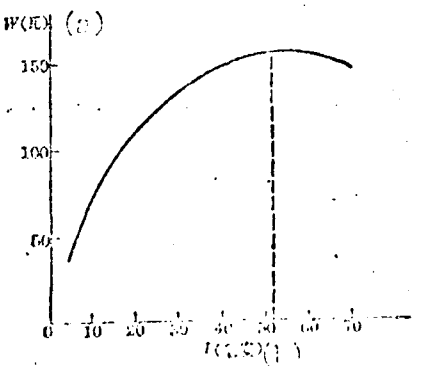

Fig. 5. [illegible]
Key: (a) [illegible]; (b) (milliamperes); (c) [illegible].

Key: (a) [illegible] (watts); (b) [illegible]; (c) [illegible].

The [illegible] results that the experiments are listed in Table 2.

Table 2

	5	10	15	20	25	30	35	40	45	50	55	60
	56.0	82.0	81.0	101	119	127	138	143	146	152	158	162
	3.7	8.2	9.5	10.4	11.5	12.0	12.5	12.8	13.0	13.0	13.0	13.0
	00	10	10	10	10	10	10	10	10	10	10	10

Key: (a) Discharge current (milliamperes); (b) Laser power (watts); (c) Melt-pool diameter (millimeters); (d) Mode.

Plot the above-mentioned experimental results and theoretical calculations onto Figure 6 for comparison. We can see that during low power periods, generally the experimental results and theoretical calculation of mode 1 at times are consistent. When the laser output power is at higher values, the experimental values are smaller than the theoretical calculations. The reason for this is that the [illegible] effect [illegible] with higher discharge currents. If the effect of [illegible] is taken into [illegible] then the [illegible] results can be [illegible] with the experimental [illegible]. [illegible]

[illegible] a resonator cavity [illegible] a round-trip cycle (Fig. 7) of [illegible] can be described by the following matrix [2]:

$$\begin{bmatrix} A & B \\ C & D \end{bmatrix} = \begin{bmatrix} 1 & 0 \\ 0 & 1 \end{bmatrix} \cdot \begin{bmatrix} \cosh\gamma L & \gamma^{-1}\sinh\gamma L \\ \gamma\sinh\gamma L & \cosh\gamma L \end{bmatrix} \cdot \begin{bmatrix} 1 & 0 \\ -\frac{2}{R_3'} & 1 \end{bmatrix} \cdot \begin{bmatrix} \cosh\gamma L & \gamma^{-1}\sinh\gamma L \\ \gamma\sinh\gamma L & \cosh\gamma L \end{bmatrix} \cdot \begin{bmatrix} 1 & 0 \\ -\frac{2}{R_2'} & 1 \end{bmatrix} \cdot \begin{bmatrix} \cosh\gamma L & \gamma^{-1}\sinh\gamma L \\ \gamma\sinh\gamma L & \cosh\gamma L \end{bmatrix} \cdot \begin{bmatrix} 1 & 0 \\ -\frac{2}{R_3'} & 1 \end{bmatrix} \cdot \begin{bmatrix} \cosh\gamma L & \gamma^{-1}\sinh\gamma L \\ \gamma\sinh\gamma L & \cosh\gamma L \end{bmatrix}$$

In the equation,

$$R_2' = \frac{R_2 d}{d - R_2\alpha_1 T_2} = \frac{2LR_2}{2L - 2MWR_2};$$

$$R_3' = \frac{R_3 d}{d - R_3\alpha_1 T_3} = \frac{2LR_3}{2L - 1.5MWR_3}$$

Assume W=150 watts, R_2'=20.10 meters, R_3'=10.08 meters, and the value of γ is approximately estimated as 1.6×10^{-3} per centimeter. Then the above-mentioned matrix value is

$$\begin{bmatrix} -0.0306 & 4.2555 \\ -0.2342 & -0.0285 \end{bmatrix}.$$

Since this optical reciprocating matrix

$$\begin{bmatrix} A & B \\ C & D \end{bmatrix} = \begin{bmatrix} 2g_1''g_2'' - 1 & 2L_c''g_2'' \\ -\frac{2}{L_c''}g_1''(g_1''g_2'' - 1) & 2g_1''g_2'' - 1 \end{bmatrix}$$

Therefore, $A=(D/2)\pm\sqrt{(D/2)^2-1}$, $g_1''g_2''=A$ and $B=2L_c''g_2''$. Since this lens series is counted from the output window, $g_1''g_2''=1$. By analysis the above condition, we derive $g_2''=0.456$ and $L_c''=4.62$ meters. L_c'' is the length of confocal two-lens chamber. By using Gaussian distribution law [3], the radius (at the 2.718 spot in the TEM_{00} mode) of 3.2-mm thickness and reflectance 2.5% mirror is 1.5 millimeters. Then,

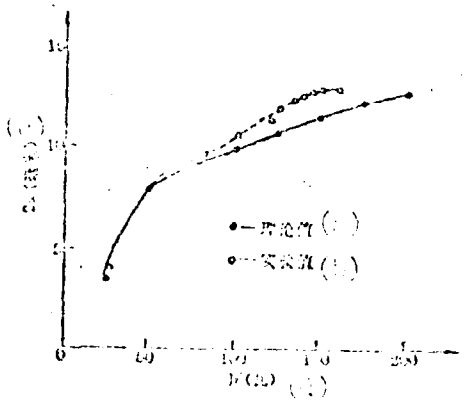

Fig. 6. [illegible] between theoretical calculation and experimental results of the laser output [illegible].
Key: (a) theoretical value; (b) experimental results; (c) (milliwatts); (d) (watts).

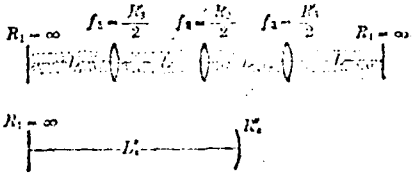

Fig. 7. One period of lens series and its equivalent two-lens chamber as the space is filled with lens-like media.

V. Discussion

If the [illegible] of a laser is relatively high and the coefficient of thermal expansion and thermal conductivity are relatively large, we cannot neglect the effect of mirror thermal deformation on laser resonator parameters. In particular, for a folded CO_2 [illegible] with output power greater than 10^3 watts, in order to commercialize the [illegible] of plane dielectric tube and mirror type pipeline chamber [illegible], the effect of mirror thermal deformation must be included in the [illegible].

FOLDED RESONATOR FOR HIGH POWER LASERS

Lei Shizhen, and Zhou Suyuqi
Shanghai Institute of Optics and Fine Mechanics, Chinese Academy of Sciences
Submitted 7 April 1980

Using ray transfer matrix, we have computed beam radii and mode volumes in the folded resonator and the dependence on mirror curvatures of resonator and the parameter α of the gas plasma negative lens. Results indicate that folded resonator configuration used in a laser with larger plasma length, not only reduces the size length of the device, but also possesses significance for obtaining stable high power output taking into account of the effect of negative plasma lens.

The folded resonator configuration is often used in some high-power lasers, such as gas dynamic laser, chemical laser, high-speed flow gas laser, dye laser, and sealed-off-enclosed high power CO_2 molecule laser. Especially for CO_2 molecule lasers, adoption of the folded chamber not only reduces the spatial length of apparatus, but the output power of the apparatus can also be higher than that without the folded configuration. In paper [1], there is a discussion on the mode volume of a resonator composed of three mirrors. However, there is no consideration given to the lens effect of the gas plasma; this is a very important factor. In high power lasers, during the operation of the apparatus, gas plasma is always used to transmit energy to the working substance molecules. But it unavoidably, in the cavity is inside the

[illegible] [illegible] sufficient [illegible] of resonator into a practically plane [illegible], [illegible] resonator configuration: loss of [illegible] power is [illegible]. [illegible] a laser resonator with relatively long fixed [illegible] length is designed. Should the mirror (for turning laser direction) be spherical or plane? What radius of curvature should be chosen? All the above-mentioned problems naturally concern comrades engaging in high-power gas laser research.

We used a three-turn sealed-and-ionized CO_2 molecule laser as an example; a light transmission matrix and an electronic digital computer were used for the numerical computation. Some resonator characteristics were discussed.

Figure 1 shows a resonator of three-turn sealed-and-ionized CO_2 molecular laser; R_1 is the spherical mirror; R_4 is the plane mirror; R_2 and R_3 are used for the turning light channel, called turning mirrors; and l_1, l_2 and l_3 are, respectively, the lengths of the three-turn discharge tube. According to the light transmission matrix, the ABCD matrix (for a single round trip of a light beam in this resonator) is:

$$\begin{pmatrix} A & B \\ C & D \end{pmatrix} = T_{11} \cdot T_{12} \cdot T_{13} \cdot T_{14} \cdot T_{15} \cdot T_{16} \cdot T_{15} \cdot T_{14} \cdot T_{13} \cdot T_{12} \cdot T_{17} \cdot T_{18} \cdot T_{19}.$$

In the equation,

$$T_{11} = \begin{pmatrix} \cosh[\alpha(l_1 - z_1)], & \alpha^{-1}\sinh[\alpha(l_1 - z_1)] \\ \alpha \sinh[\alpha(l_1 - z_1)], & \cosh[\alpha(l_1 - z_1)] \end{pmatrix};$$

$$T_{12} = \begin{pmatrix} 1, & 0 \\ -2/R_2, & 1 \end{pmatrix};$$

$$T_{13} = \begin{pmatrix} \cosh(\alpha l_2), & \alpha^{-1}\sinh(\alpha l_2) \\ \alpha \sinh(\alpha l_2), & \cosh(\alpha l_2) \end{pmatrix};$$

$$T_{14} = \begin{pmatrix} 1, & 0 \\ -2/R_3, & 1 \end{pmatrix};$$

$$T_{12}\left(\begin{array}{cc}\cosh(al_2), & a^{-1}\sinh(al_2)\\ a\sinh(al_2), & \cosh(al_2)\end{array}\right)$$

$$T_{23}\left(\begin{array}{cc}1, & 0\\ -2/R_2, & 1\end{array}\right);$$

$$T_{31}\left(\begin{array}{cc}\cosh(al_3), & a^{-1}\sinh(al_3)\\ a\sinh(al_3), & \cosh(al_3)\end{array}\right);$$

$$T_{14}\left(\begin{array}{cc}1, & 0\\ -2/R_1, & 1\end{array}\right);$$

$$T_{10}\left(\begin{array}{cc}\cosh(az_1), & a^{-1}\sinh(az_1)\\ a\sinh(az_1), & \cosh(az_1)\end{array}\right).$$

The radius ω of the light spot of the beam in the cavity is

$$\omega^2=\frac{2\lambda B}{\pi}\Big/\sqrt{1-(A+D)^2}$$

The volume of the laser mode is

$$V=\pi\int_0^l\omega^2(z)dz$$

In the equation, λ is wavelength; a is the diametrically distributed parameter of refractivity ($a=\sqrt{\bar{n}_2^2-\bar{n}_0^2}$; the diametrical distribution of refractivity n takes the form of $n=n_0+(1/2)n_2r^2$). A TQ-16 electronic computer was used for the numerical computation.

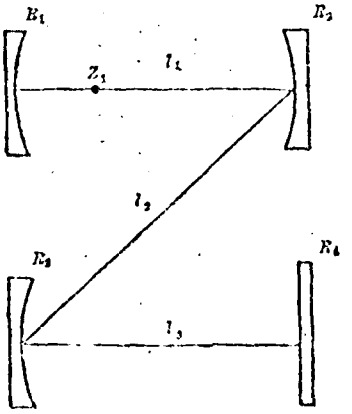

Fig. 1. Folded cavity ring resonator.

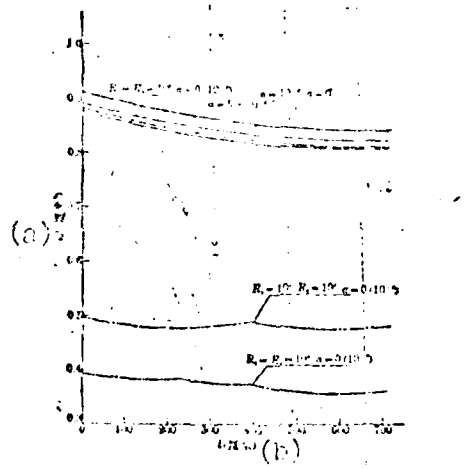

Fig. 2. Distribution of light-spot radii along the length of chamber in a folded chamber: ——— not folded; -.-.-.- folded.
Key: (a) Some centimeters; (b) Centimeters.

Figures 3 through 5 show the relationship between the radius of curvature of the [illegible] and the radius of the spot on the mirror and value V of [illegible] for different α. Figures 3 and 4 show the variations in the radius of curvature of the [illegible] light-spot radius and mode value V for fixed [illegible] 10^{4} centimeters, [illegible] centimeters, L_1=200 centimeters, and [illegible].

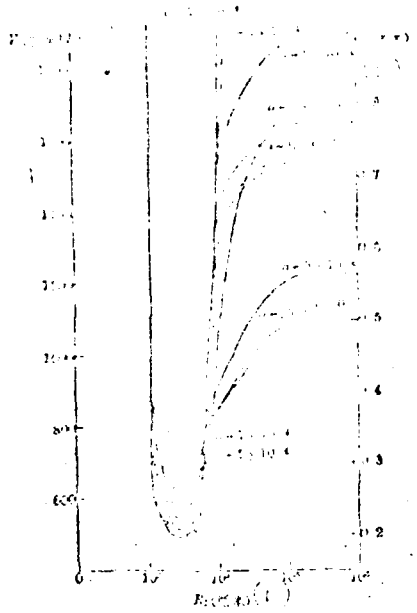

Fig. 3. [illegible] Key: (1) [illegible]; (2) [illegible].

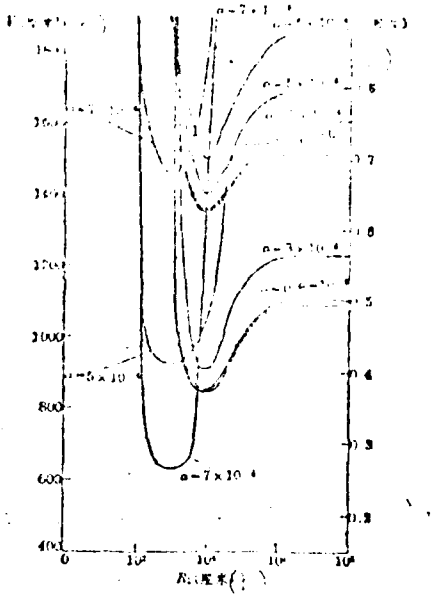

Fig. 4. [illegible] Key: (a^3) (cubic centimeters); (b) (centimeters).

Apparently, [illegible] are the same; the mode volume is very small at $R_3=10^2$. [illegible] the emitting of the same R_3 value, the mode volume at $R_2=10^8$ cm is [illegible] $R_2=10^4$ cm. However, when the value of a is relatively large ($a=[illegible]$), it is easier to let the mode volume of resonator approach infinity; i.e., the [illegible] tends to enter the high-loss zone of light output power. According to the results from Figures 3 and 4, when $R_2=10^4$ and $a=5\times10^{-4}$, even R_3 is no greater than 10^2 cm; the resonator is still in the low-loss region. However, when $R_2=10^8$ cm, R_3 is only limited to a value in the vicinity of 10^4 cm and the consumption of light power in the cavity is then relatively low. In addition, we can see from Fig. 3 that if R_2 changes from 10^4 to 10^8 cm and the change of mode volume is small, R_3 is between 2×10^2 cm. However, the stability requirement of the [illegible] (i.e., a region of curvature) is higher since any [illegible] can [illegible] the [illegible] of the [illegible] power. From the [illegible] we can see that the mode [illegible] value of the resonating mirror can be [illegible] R_2.

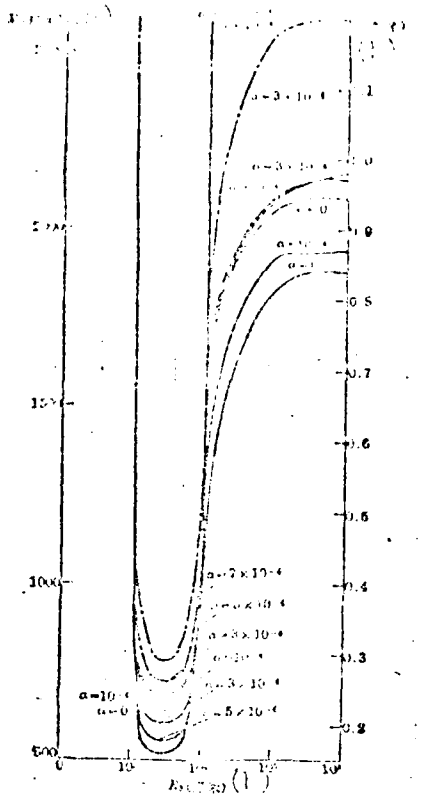

$E_3 \sim V$ ——; $E_3 \sim a$ - - -

Fig. 4. Relationship between E_3 on one hand, and light-guide radius or mode volume on the other (logarithmic coordinates). Key: (a) (cubic centimeters); (b) (centimeters).

We can see from the results in Figures 3 to 5 that because the condition of the same radius of curvature of the mirrors at both resonator ends, the mode volume of the folded chamber is smaller than that for the nonfolded chamber. From this point, adoption of the folded resonator configuration does not tend to increase the power of the laser. However, as there is a possible loss effect in the laser working medium, if the folded resonator configuration is not adopted, the loss of light power in the laser working medium (due to an overlapped cumulative effect) will be still limited to a lower level because of the comparatively small mode volume (irrespective of the a value). We can see from Figure 5 that by applying the folded resonator for

[illegible] this point is also proved experimentally. The following table shows the output power for different radii of curvature in a three-turn resonator.

R_1([illegible])(a)	1.8×10^4	1.8×10^4	1.25×10^4
R_2([illegible])(a)	∞	10^4	∞
R_3([illegible])(a)	∞	10^4	10^4
R_4([illegible])(a)	∞	∞	∞
[illegible](b)	50	50	250~300

Key: (a) Centimeters; (b) Output power (watts).

When the first set of data is adopted in a resonator, the mode volume is greater than for the third-set of data. However, the power obtained by using the third-set data is much greater than for the first set. From the calculated results listed in Fig. 5, for the resonator of the first-set data, the mode volume is too large; i.e., the loss is too high. For the resonator of the second-set data, the corresponding mode volume is too small, so this is also not suitable. Hence, the laser output power is also the lowest.

Figure 6 shows the relationship among the beam light spot radius, mode volume, and α value of the laser working medium. We can see from the figure that the larger the radius of curvature of the turning mirror, the smaller the allowable range of α values. However, the α value is determined by the laser working medium; the larger

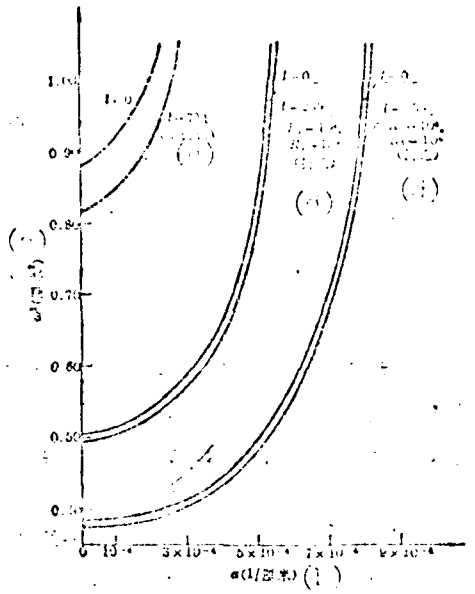

Fig. 6(a). Relationship between light-spot radius and α: (in the figure, curves for $l=0$ and $l=711$, 235 represent, respectively, light-spot radius of mirror R_1, and the values of light spots at distances of 711 and 235 cm from mirror R_1)
Key: (a) (square centimeter); (b) (1/centimeter); (c) (not folded); (d) (folded).

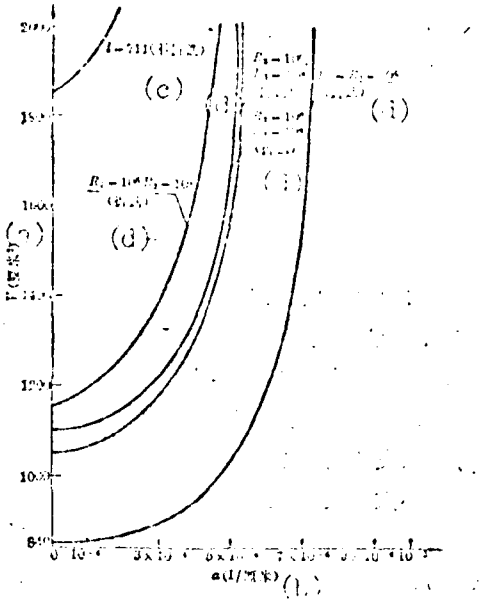

Fig. 6(b). Relationship between mode volume and α.
Key: (a) (cubic centimeter); (b) (1/centimeter); (c) (not folded); (d) (folded).

Therefore, when designing a resonator, it is appropriate to choose spherical mirrors as light-turning mirrors; as for the R_2 and R_3 values, they are related to the length of each folded element. By using the light transmission matrix and its standard calculation procedure, a comparison calculation can be had to the mode volume and in-chamber energy flux, suitable values can be chosen.

1. [illegible]
2. [illegible]
3. [illegible]

A COPPER VAPOR LASER

Liang Paogen, Jing Chunyang, Zhang Guiyan,
Yin Xanhua, Cong Yunching, and Han Sanchen

Shanghai Institute of Optics and Fine Mechanics, Chinese Academy of Sciences

Submitted 30 November 1979

With copper vapor or copper halide vapor as laser medium, excited by high repetition frequency resonance Blumlein discharge circuit, laser output are obtained at 5106 Å and 5782 Å. For charge capacitance of 1.5 nf, charge voltage of 6000 V and a repetition rate of 16 KHz, the average output laser power is 1.2 W.

1. Introduction

Among pulsed metal vapor lasers, the atomic copper vapor laser is a typical type. The copper vapor laser requires relatively high working temperatures and excitation with short pulses; there are a series of technical difficulties. In the past, people were not interested in the development of copper vapor lasers. Until 1970 after Soviet researchers successfully manufactured implements with an average power of 15 watts [1], the general attitude was changed in a way of improving and developing copper and other metal vapor lasers. In 1973, an American used copper halide to replace copper as the working medium, considerably reducing the required working

[illegible]

C. [illegible] Transmission

Copper halide vapor is adopted as the laser working medium. It is known generally that metal vapor has very low vapor pressure at room temperature and copper is one such metal. However, for resonance self-trapping, the minimum vapor density of 10^{13} cm^{-3} is required for a 1-cm diameter tube. This vapor density can only be attained at high temperatures. For copper halides, the temperature required to attain this vapor density is 300~600°C as we applied discharge self-heating method to carry it out. For pure copper, it is required to heat to above 1500°C. We used an electric furnace outside a discharge tube to first heat the copper to 1000 °C. Then after discharge, the pure copper heated spontaneously to a high temperature above 1500°C.

An quartz tube of ϕ8~12 and a ceramic aluminite tube were used to construct the discharge tube; the distance between electrodes is 250~300 mm; connections between cerium tungsten electrode and quartz tube employed molybdenum seals. Two terminals of discharge tube were ground into a quartz Brugs angle. In a copper halide vapor laser, copper halide was placed in a side tube at a middle of discharge tube. For a pure copper vapor laser, the copper powder is uniformly placed axially along the ceramic aluminite tube; in the tube 20 torr of neon is filled as a buffer gas. The distance zone uses a vacuum quartz sleeve or asbestos cloth as insulation.

The resonator is composed of a mirror of multilayer medium film (reflectivity of curved mirror is 100% total reflection to 5106 Å and a reflectivity of copper is (for a plane multilayer medium)

[illegible] only [illegible] [illegible] coil [illegible] in the circuit [illegible] current wave[illegible] (Fig. 3). [illegible] The measurement of voltage and current waveform [illegible] when the discharge capacitance was at 3 nanofarads, charge voltage at 3500 volts, pulse repetition frequency at 10 kilohertz, and an 4.8x250 laser tube was used.

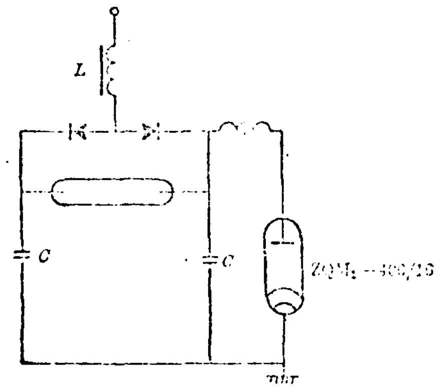

Fig. 1. Schematic diagram of charge and discharge circuit.

Fig. 2. Voltage waveform at charge and discharge: time scale at 0.1 millisecond per centimeter.

Fig. 3. Charge current waveform: amplitude at 10 volts per centimeter and time scale at 50 nanoseconds per centimeter.

[illegible] Moreover, at the [illegible] Å, [illegible] Å laser output power [illegible].

For copper bromide vapor laser, the average laser output power is 2.5 watts for an internal laser tube diameter of 32 pole-to-pole distance of 50 millimeters, charge capacitance at 1.5 nanofarads, charge voltage of 6000 volts, and pulse repetition frequency at 10 kiloherts.

For a pure copper vapor laser (ϕ8x250), the average laser output power is 150 milliwatts with charge capacitance at 2 nanofarads, charge voltage at 6000 volts, and pulse repetition frequency at 10 kiloherts.

A circular-disk monochromator (with removal of a narrow exit seam) was used for photographing 5106Å and 5782Å spectral lines (Fig. 4). In the figure, the mercury spectral line is used as a comparison line.

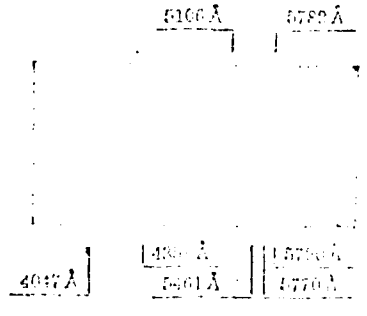

Fig. 4. Light spectral lines for 5106Å and 5782Å (the mercury line is used as a comparison line).

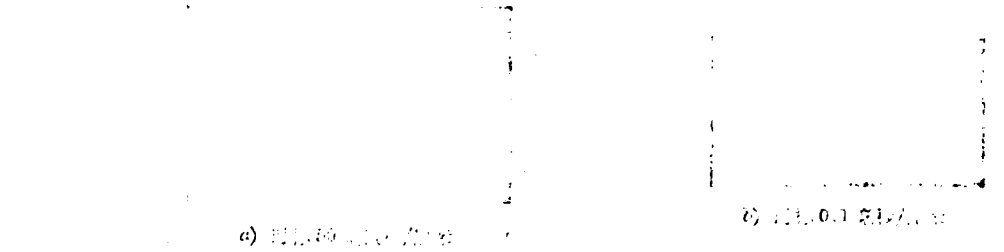

Fig. 5. [illegible] laser waveform: (a) Time scale at 50 microseconds per centimeter; (b) Time scale at 0.1 millisecond per centimeter.

During the experiment it was found that the incessant wearing of copper bromide during the working process is an important factor why this type of laser apparatus has a short life-span. Under the precondition of correctly controlling temperatures, an increase of the filling medium is the most direct method of extending the laser emission service life. The filling medium of our laser ($8x250) amounted to about 2 grams and the stabilized light-emitting duration was more than 15 hours. During the later period of the service life of this type of laser, often the (relatively intensive) discharge channel is quivering, bending, and narrowing; this is relatively closely related to the electrophoresis effect during the discharge process. The electrophoresis effect causes the density of copper particles to gradually decrease in the discharge channel. In a situation where there is no timely supply of the filling medium, E/N gradually increases, causing an unstable discharge electrode, or even violently extinguishing it.

[illegible]

J. [illegible], [illegible], [illegible]: [illegible] V [illegible], 1970, 16, No. 1, 40.

SCIENCE NOTES: ULTRAVIOLET PRE-IONIZATION DISCHARGE PUMP ArF LASER

Fu Shufen, Chen Jiansen, and Liu Miaohong
Shanghai Institute of Optics and Fine Mechanics, Chinese Academy of Sciences

On an ultraviolet pre-ionization high-gas-pressure laser, we successfully achieved ArF laser oscillation. The experimental installation is shown in Fig. 1. The discharge chamber is a nylon circular cylinder one meter long, with an internal diameter of 76 millimeters. A thin-shell aluminum flange was used to directly connect an optical resonator sheet onto two cylinder terminals. By use of an elastic (deformation adjustment) cavity sheet of the flange, it is conveniently adjusted with stable characteristics. In addition, the effect of absorption by the atmosphere layer (in the external cavity type apparatus) on laser wavelength can be avoided.

The main discharge electrode is brass; its surface is cylindrical with 8.1 millimeter. This round, smooth electrode with small radius can lead to uniform discharges and to strengthen the density of the excitation power. The parallel-plate capacitor consists of two 0.5-mm-thick electrolytic copper foils, with a molded 0.5-mm polyester thin film. The main-pole discharge is upon the electrode s

[illegible] circuit of [illegible] is shown in Fig. 2.

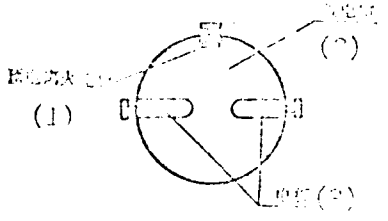

Fig. 1. [illegible] of ultraviolet pre-ionization ArF laser.
Key: (1) Pre-ionization spark plate; (2) Discharge chamber; (3) Electrode plate.

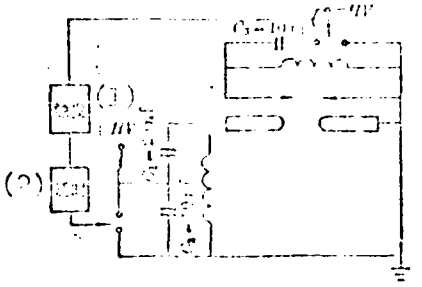

Fig. 2. Equivalent circuit of laser system.
Key: (1) Triggering; (2) Delayed.

When the main discharge and charge are 20 kilovolts, the total input energy is 6 joules. The delay time between main discharge and pre-ionization is a very important parameter; the selection of the best delay time relies on the pre-ionization capacitance, charge voltage, constituents of gas filled, and gas pressure.

The gas mixture is NF_3:Ar:He=0.2%:12%:87.8%; laser outputs were obtained at a total gas pressure of 1.5~2.5 atmospheric pressures. Figure 3 shows a blackness curve of the ArF laser spectrum photographed with a 2-meter grating spectrograph; the total width at half intensity is 3A.

Compared with XeF and KrF, the service life of the ArF laser is considerably shorter; this is probably because of light-absorbed impurities in the discharge. In order to [illegible] long service life and

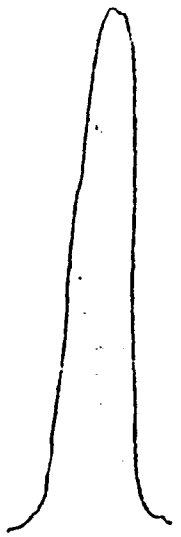

Fig. 3. Blackness curve of ArF laser spectrum

The authors express their gratitude to Fudan University and Dalian Institute of Chemistry and Physics for providing gas used in the experiment.

LITERATURE

1. Furukawa, R., et al: APPL. PHYS. LETT., 1976, 29, 707.

2. Lowe, T. E., et al.: APPL. PHYS. LETT., 1978, 32, 171.

EXPERIMENTS AND RESEARCH OF ELECTRON BEAM CONTROL XeCl QUASI-MOLECULE LASER

Hong Pu

Institute of Electronics, Chinese Academy of Sciences

We built a large volume (10 liters) electron beam lateral pump and electron beam-controlled discharge laser; Fig. 1 shows the schematic diagram of the laser structure.

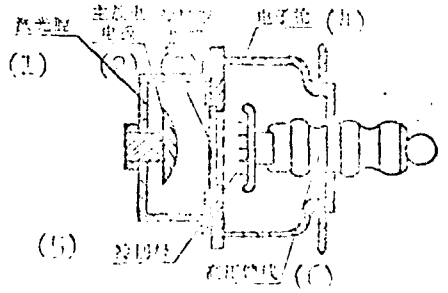

Fig. 1. Schematic diagram of structure.
Key: (1) Laser chamber; (2) Main discharge electrode; (3) Polyimide film; (4) Electron gun; (5) Cold cathode; (6) High transparency metal film.

[illegible]

[illegible] plate, whose transm[illegible] than plexi[illegible]. [illegible] to holders. [illegible] with [illegible] of 8 [illegible]. The mirrors have two standard diameters which are 5.7 centimeters and 12 centimeters respectively. The mirrors are coated with a multi-layer-medium film, mirror spacing is 1.5 meters. One mirror has a total reflection of 3080Å (reflectivity over 99 percent) and the other mirror has a reflectivity of 82 percent, constituting an optical resonator.

The anode of the laser resonator is a solid aluminum flat electrode. There are two values for the distance between two electrodes. When d=5.7 centimeters, the discharge volume of the laser resonator is 5.7 liters; when d=9 centimeters, the discharge volume of the laser resonator is 9 liters. The power source for the main discharge is composed of four parallel capacitors of 0.5 microfarad and 50 kilovolts.

In the experiment, HCl was used as the chlorine source. Ar was used as a diluting agent; the mixing ratio is Ar/Xe/HCl=95.8/3.8/0.4. The total pressure was one atmospheric pressure. At the side of the total reflection mirror (rate of transparency 0.2 percent) of the laser resonator; the laser spectrum was obtained by photography. When a low-pressure mercury lamp is used as standard spectrum, Fig. 2 shows the photographed spectral lines and Fig. 3 shows the spectrum density curve of the measured. From Fig. 3, five laser spectra are clearly seen with wavelengths at 3080 Å and 3093 Å.

[illegible] 0.5 m from the laser output window. [illegible] light spot is relatively uniform. [illegible] different distances, we can calculate that the divergence angle of the laser beam is 2 milliradians.

Fig. 2. XeCl laser spectral lines.

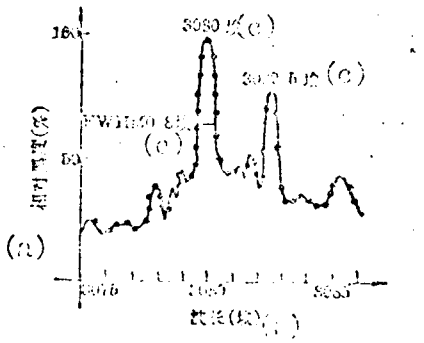

Fig. 3. Distribution curves of XeCl laser spectrum density. Key: (1) [illegible]; (2) Wavelength (Å); (3) Å.

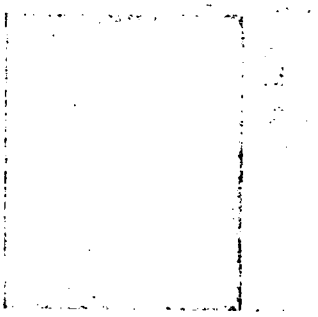

Fig. 4. Laser spot (at 0.48 meter from the output window).

The maximum output energy is 1 joule. During experiments, the output [illegible] At that time, the effective [illegible] was 1.6 liters; therefore, the output [illegible] was 0.6 joule per liter; the conversion [illegible] energy was 0.64 percent.


FILMED
4
8